Stress tensor and viscosity of water: Molecular dynamics and generalized hydrodynamics results

Davide Bertolini
Istituto di Fisica Atomica e Molecolare del CNR, Via del Giardino 7, I-56100 Pisa, Italy

Alessandro Tani*
Dipartimento di Chimica e Chimica Industriale, Universitá di Pisa, Via Risorgimento 35, I-56126 Pisa, Italy
(Received 5 August 1994; revised manuscript received 15 March 1995)

The time correlation functions (CF's) of diagonal and off-diagonal components of the stress tensor of water have been calculated at 245 and 298 K in a molecular dynamics (MD) study on 343 molecules in the microcanonical ensemble. We present results obtained at wave number $k=0$ and at a few finite values of k, in the atomic and molecular formalism. In all cases, more than 98% of these functions are due to the potential term of the stress tensor. At $k=0$, their main features are a fast oscillatory initial decay, followed by a long-time tail more apparent in the supercooled region. Bulk and shear viscosities, calculated via Green-Kubo integration of the relevant CF at $k=0$, are underestimated with respect to experimental data, mainly at low temperature, but their ratio (≈ 2) is correctly reproduced. Both shear and bulk viscosity decrease as a function of k, the latter more rapidly, so that they become almost equal at ≈ 1 Å^{-1}. Also, both viscosities drop rapidly from their maximum at $\omega=0$. This behavior has been related to the large narrowing observed in the acoustic band, mainly in the supercooled region. The infinite frequency bulk and shear rigidity moduli have been shown to be in fair agreement with the experimental data, provided the MD value used for comparison is that corresponding to the frequency range relevant to ultrasonic measurements. The MD results of stress-stress CF's compare well with those predicted by Bertolini and Tani [Phys. Rev. E **51**, 1091 (1995)] at $k=0$, by an application of generalized hydrodynamics [de Schepper *et al.*, Phys. Rev. A **38**, 271 (1988)] in the molecular formalism, to the same model of water (TIP4P) [Jorgensen *et al.*, J. Chem. Phys. **79**, 926 (1983)]. These CF's are essentially equal in the atomic and molecular formalism, the only minor difference being restricted to the high frequency librational region of the shear function. By a comparison of atomic and molecular results, we show here that neglecting libration has no effect on the density-density and longitudinal current CF's and very little effect on transverse properties. On the other hand, this study points out the importance of including the oscillation in the nearest-neighbor cage in the memory function of the longitudinal and transverse current CF. The oscillatory local motion turns out to play an important role in all CF's and hence contributes significantly to the value of viscosity and of rigidity moduli.

PACS number(s): 61.20.−p, 61.25.−f, 62.60.+v

I. INTRODUCTION

Recently [1], generalized hydrodynamics [2] has been applied to the transferable intermolecular potential with four points (TIP4P) model of water [3] at 245 and 298 K. The density-density, energy-density, and the energy-energy, in addition to longitudinal and transverse current time correlation functions, have been calculated at several values of wave numbers k. With this information, it has been possible to predict [1] the behavior of the time correlation function CF of the diagonal components of the stress tensor [2,4,5] in the $k=0$ limit, and to compute shear η and longitudinal viscosity $\eta_L \equiv \frac{4}{3}\eta+\zeta$. The calculation [1] is based essentially on an extrapolation to $k=0$ of the parameters that describe the behavior of the memory kernel of the density-density, or of the longitudinal current CF. Though not explicitly considered in [1], the CF of the off-diagonal components of the stress tensor can be obtained in the same way from the data on the CF of the transverse current.

The main features of the predicted stress-stress autocorrelation functions are a rapid initial drop with an oscillation of frequency 45–50 THz (1 ps^{-1}=1 THz) and a long-time tail. The former oscillatory mode is generally related to the translational motion of the tagged molecule in the nearest-neighbor case and can be observed in the spectrum of the velocity autocorrelation function (ACF). Its average behavior and its dependence on the number of hydrogen bonds has been discussed elsewhere [6]. The latter feature, the long-time tail, also present in simple liquids [7–9], has been shown [1] to determine the shape of the dispersion curve of the acoustic mode.

The present paper serves two main purposes. First, to study, by equilibrium molecular dynamics (MD) techniques, the ACF of stress tensor fluctuations both in the molecular and atomic formalism [10–12], and to recalculate density, longitudinal and transverse current ACF's in the atomic formalism. The latter functions were computed in [1] in an "effective" molecular formalism, whereby

*Author to whom correspondence should be addressed.

all phase factors appearing in the CF's were relevant to the center of mass, although energy was necessarily calculated including all site-site contributions, as required by the TIP4P model. Thus, only rotational kinetic terms were neglected. As discussed in [1], this treatment relies on the time-scale separation between librational and center of mass motions and on the larger size of the potential energy terms compared to the kinetic ones.

Here most of the attention is devoted the stress-stress ACF and viscosity at $k=0$ and at 298 and 245 K. Moreover, the k dependence of these properties, again in both formalisms, has also been analyzed. The (k,ω)-dependent viscosities have been used to rationalize the large narrowing of the acoustic band [1], which, together with the anomalous sound dispersion, have been the subject of extensive debates over the last decade [13].

Our second principal goal is to provide "experimental" data to test the theoretical prediction [1] on the stress-stress autocorrelation function. Through this comparison, the contribution of water dynamics to viscosity as a function of the characteristic time scale has been determined. In particular, the role of librational dynamics, not included in the theoretical model [1], on viscosity and rigidity moduli has been tested. The latter are compared to experimental measurements in the frequency range they both can cover.

This paper is organized as follows. Section II outlines the theoretical approach used to analyze the simulation results concerning the stress tensor. The MD results for the relevant time correlation functions in the atomic and molecular formalisms are reported in Sec. III A. Section III B discusses the comparison of MD data with those predicted by a slightly modified version of the model introduced in [1] for the time dependence of transport parameters. The latter is required to improve the description of the transverse currents. The same section also presents results for vortex viscosity and bulk and shear rigidity moduli. A summary of the main results and conclusions is given in Sec. IV.

II. THEORETICAL BACKGROUND

The theory introduced in [2] and applied to water [1] leads to a set of relations for the Laplace transform of the CF of the collective dynamical variables of interest. The general expressions that are used in the following are Eqs. (3.23)–(3.28) of Ref. [1]. They define $G_{ij}(k,t)$, a set of orthonormal linear combinations of the CF's $F_{ij}(k,t)$, with $i,j=1,2,3,4,5$. These numbers label density, longitudinal velocity, energy, stress tensor, and longitudinal heat flux, respectively. The $G_{ij}(k,t)$'s turn out to be more convenient than $F_{ij}(k,t)$ from the point of view of the theoretical analysis and also have a simpler physical meaning.

The general equations (3.23)–(3.28) of [1] become much less complex when $\gamma(k)=c_P(k)/c_V(k)\rightarrow 1$ and $|z_{q\sigma}(k,z)|\rightarrow 0$. The latter condition amounts to neglecting the correlations between the stress tensor and the longitudinal heat flux. For water described by the TIP4P model, we found [1] that these conditions are satisfied to a good approximation for $k<1$ Å^{-1} both at 245 and 298 K. Hence, we can use a set of simplified expressions [Eqs. (4.19)–(4.23) of [1]], i.e., in the case of the diagonal components of the stress tensor

$$\tilde{G}_{44}(k,z)\cong\frac{[z^2+f_{un}(k)^2]}{[z+z_\sigma(k,z)][z^2+z_\phi(k,z)z+f_{un}(k)^2]}\ , \tag{2.1}$$

where

$$z_\phi(k,z)\cong\frac{f_{u\sigma}(k)^2}{[z+z_\sigma(k,z)]}\equiv f_{u\sigma}(k)^2\tilde{n}_\sigma(k,z)\ . \tag{2.2}$$

The generalized frequencies $f_{un}(k)$ and $f_{u\sigma}(k)$ can be obtained [see Eqs. (2.28) in Ref. [2]] from the initial values $[V_{ij}(k)=F_{ij}(k,0)]$ of the $F_{ij}(k,t)$.

The generalized transport parameters $z_\sigma(k,z),z_q(k,z),z_{q\sigma}(k,z)$ [1,2], which determine the k and ω dependence of generalized viscosity $\eta(k,\omega)$, thermal conductivity $\lambda(k,\omega)$, and ratio of specific heats $\gamma(k,\omega)$, must be described by models at the present state of the theory. In the case of water, the frequency dependence of $z_{q\sigma}(k,z)$ can be neglected and $\gamma\cong 1$, at least for $k<1$ Å^{-1}.

The Laplace transform of the transverse current $C_\perp(k,t)$ can be written as [4,5,7]

$$\tilde{C}_\perp(k,z)=\frac{C_\perp(k,0)}{z+\omega_\perp(k)^2\tilde{n}_\perp(k,z)}\ , \tag{2.3}$$

where

$$\omega_\perp(k)^2=-\lim_{t\rightarrow 0}\frac{\partial^2[C_\perp(k,t)/C_\perp(k,0)]}{\partial t^2}\ . \tag{2.4}$$

$\tilde{n}_\sigma(k,z)$, and then $n_\sigma(k,t)$ can be obtained from a model for $z_\sigma(k,z)$ and a fit of the transforms of the normalized density-density or longitudinal current CF, or a combination of these two CF's, as explained in [1]. Analogously, a fit of the transverse current CF according to Eq. (2.3) can give $\tilde{n}_\perp(k,z)$ and $n_\perp(k,t)$.

In the time domain, when the above conditions $\gamma(k)=c_P(k)/c_V(k)\rightarrow 1$ and $|z_{q\sigma}(k,z)|\rightarrow 0$ hold, $G_{44}(k,t)$ can be written

$$G_{44}(k,t)\cong\frac{V_{44}(k)F_{44}^{(N)}(k,t)+\dfrac{V_{22}^2}{S(k)}[G_{11}(k,t)-2G_{22}(k,t)]}{\left[V_{44}(k)-\dfrac{V_{22}^2}{S(k)}\right]}\ , \tag{2.5}$$

where $F_{44}^{(N)}(k,t)$ is the normalized CF of the diagonal components of the stress tensor. In the $k=0$ limit, the decay rates of $G_{11}(k,t)$ and $G_{22}(k,t)$ tend to vanish, i.e., $G_{11}(k\rightarrow 0,t)=G_{22}(k\rightarrow 0,t)=1$ at every t, so that $F_{44}^{(N)}(k,t)$ behaves as $G_{44}(k,t)$.

Moreover, in the same $k=0$ limit, $G_{44}(k,t)$ becomes equal to $n_\sigma(k,t)$ as $f_{un}(k)$ and $f_{u\sigma}(k)$ go to zero with k in Eq. (2.1). Hence,

$$n_\sigma(k\to 0,t)\cong G_{44}(k\to 0,t)\cong F_{44}^{(N)}(k\to 0,t) \equiv \frac{F_{44}(k\to 0,t)}{F_{44}(k\to 0,0)} . \quad (2.6)$$

A similar relation holds for the CF of the off-diagonal components of the stress tensor [7], hereafter referred to as $F_{44}^{(\perp)}(k\to 0,t)$,

$$n_\perp(k\to 0,t)=F_{44}^{(\perp N)}(k\to 0,t)\equiv \frac{F_{44}^{(\perp)}(k\to 0,t)}{F_{44}^{(\perp)}(k\to 0,0)} . \quad (2.7)$$

Equations (2.6) and (2.7) allow us to compare $n_\sigma(k\to 0,t)$ and $n_\perp(k\to 0,t)$, computed directly at $k=0$ with those obtained in [1] from a fit of the transforms $\tilde{G}_{11}(k,z)$ [or $\tilde{G}_{22}(k,z)$] and $\tilde{C}_\perp(k,z)$, and an extrapolation to $k=0$ of the best fit parameters.

From these transforms, longitudinal and shear viscosity could be calculated in [1]. These results will be compared with that obtained here through the Green-Kubo relations

$$\eta_L \equiv \tfrac{4}{3}\eta+\zeta=\frac{\rho M}{k_B T}\int_0^\infty F_{44}(0,t)dt \quad (2.8)$$

and

$$\eta=\frac{\rho M}{k_B T}\int_0^\infty F_{44}^{(\perp)}(0,t)dt , \quad (2.9)$$

where ρ is the average mass density and M the molecular mass.

III. RESULTS AND DISCUSSION

A. "Atomic" and "molecular" correlation functions

In the case of polyatomic fluids, the density, the longitudinal and transverse current, the stress tensor, and the longitudinal heat flux CF's can be calculated in two different ways, using either the "atomic" or the "molecular" expression [10–12]. It has been shown [14] that both formalism lead to identical values of transport coefficients and pressure, despite differences in the time dependent CF's.

A test run of 40 000 steps at 245 K has been performed where density-density and longitudinal and transverse current ACF's have been calculated both in the "molecular" (m) and "atomic" (a) formalism at $k=0.288$, 0.498, and 0.705 Å^{-1}. The expressions used to calculate density-density and longitudinal and transverse current ACF's are straightforward extensions of the definitions for the simple liquid. The difference between "atomic" and "molecular" results for the density-density, the longitudinal and transverse currents ACF's are too small to be observed on the scale of ordinary figures, so we do not show them here (see [1]). This substantial identity supports the validity of the "effective" molecular approach adopted in [1] to apply extended hydrodynamics to water and outlined in the Introduction.

Both formalisms have also been applied to calculate the stress tensor at $k=0$ as follows [14,15]:

$$\sigma^{(m)}(t)=\sum_\alpha \mathbf{v}_\alpha\mathbf{v}_\alpha+\frac{1}{M}\sum_{\alpha<}\sum_\beta(\mathbf{R}_\alpha-\mathbf{R}_\beta)\sum_i\sum_j \mathbf{f}_{i\alpha j\beta} , \quad (3.1)$$

$$\sigma^{(a)}(t)=\frac{1}{M}\left\{\sum_\alpha\sum_i m_i\mathbf{v}_{i\alpha}\mathbf{v}_{i\alpha}+\sum_{\alpha<}\sum_\beta\sum_i\sum_j(\mathbf{r}_{i\alpha}-\mathbf{r}_{j\beta})\mathbf{f}_{i\alpha j\beta} + \sum_\alpha\sum_{i<}\sum_k(\mathbf{r}_{i\alpha}-\mathbf{r}_{k\alpha})\mathbf{g}_{i\alpha k\alpha}\right\} , \quad (3.2)$$

where $\mathbf{v}$, $\mathbf{r}$, and $\mathbf{f}$ are velocity, position, and (intermolecular) force vector for an atom (Latin index) of a molecule (Greek index), while M (m) is the molecular (atomic) mass. The $\mathbf{g}$ are intramolecular constraint forces [14]. The average of the CF's of diagonal components of $\sigma(t)$ gives $F_{44}(0,t)$, while that of off-diagonal components $F_{44}^{(\perp)}(0,t)$ are

$$F_{44}(0,t)=\frac{1}{3}\left\langle\sum_\alpha\sigma^{\alpha\alpha}(0)\sigma^{\alpha\alpha}(t)\right\rangle , \quad (3.3)$$

$$F_{44}^{(\perp)}(0,t)=\frac{1}{6}\left\langle\sum_{\alpha,\beta\neq\alpha}\sigma^{\alpha\beta}(0)\sigma^{\alpha\beta}(t)\right\rangle . \quad (3.4)$$

As usual, in all correlations of diagonal components [Eq. (3.3)] the average value PV/M has been subtracted.

The generalization of Eq. (3.2) to finite k's can be obtained from the following expression for the average of the off-diagonal components (the analogous for the diagonal components is obtained replacing the cross products with the dot products):

$$\sigma^{(a\perp)}(k,t)=\frac{1}{M}\sum_\alpha\sum_j\left\{m_j\left[\frac{\mathbf{k}}{k}\times\mathbf{v}_{j\alpha}\right]^2 + \frac{i}{k}\left[\frac{\mathbf{k}}{k}\times\mathbf{F}_{j\alpha}^{(\mathrm{tot})}\right]\right\}e^{i\mathbf{k}\cdot\mathbf{r}_{j\alpha}} , \quad (3.5)$$

where $\mathbf{F}_{j\alpha}^{(\mathrm{tot})}$ is the total force (intermolecular plus constraint) acting on atom j of molecule α.

The "atomic" stress tensor is symmetric, as all forces are central forces. However, the "molecular" stress tensor can, in principle, be asymmetric [10–13]. In fact, as discussed by Olmsted and Snider [10], the total force, and mainly its Coulomb part in our case, is not directed along the line of the molecular center of mass. This produces a torque that is responsible for the small asymmetry of the "molecular" stress tensor. The ACF of the antisymmetric part of the tress tensor is related to vortex viscosity η_r, which will be discussed in the following section.

Equation (3.5) has been used at the same k values where the density and currents CF's have been studied. The functions shown in Fig. 1, where the CF of the diagonal components of the stress tensor is compared at $k=0$ and $k=k_{\min}=0.288$ Å^{-1}, show that the "atomic" and "molecular" results coincide in this case. The data at $k=0$ have been obtained from the definitions (3.1) and (3.2), while the "molecular" one, at $k=k_{\min}$, from the second time derivative of the molecular longitudinal current ACF, according to the conservation law. The latter has also been used as a check of the independent

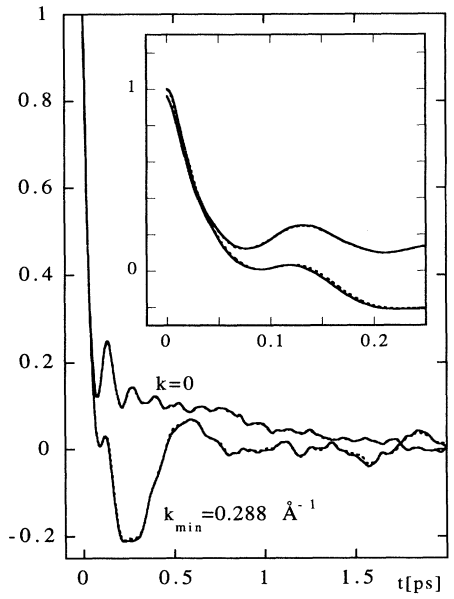

FIG. 1. Normalized ACF of the diagonal components of the stress tensor at 245 K. The full curves are "molecular" results and the dotted curves are "atomic" results. The $k=0$ data have been obtained from Eqs. (3.1) and (3.2), while that at $k=0.288$ Å^{-1} from Eq. (3.5) ("atomic" ACF) and from the conservation law ("molecular" ACF). The inset shows an enlarged view of the short-time region. The ACF's are averaged on the three diagonal components for a 100-ps run.

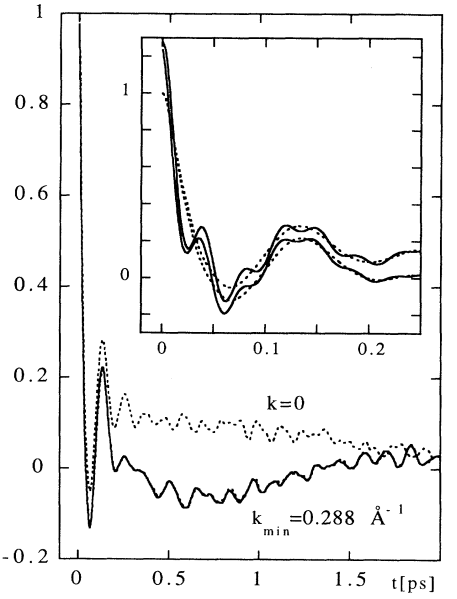

FIG. 2. "Atomic" ACF of the off-diagonal components of the stress tensor at 245 K. At $k=0.288$ Å^{-1} also the second derivative of the ACF of the atomic transverse current is reported (full curve). The "molecular" results are shown in the inset and have been normalized on the corresponding "atomic" functions.

calculation of the "atomic" $F_{44}(k,t)$ at all finite k's [Eq. (3.5)]. However, the "molecular" and "atomic" ACF's for the off-diagonal components of the stress tensor (Fig. 2) differ in the short-time region, shown in the inset, where the librational dynamics is visible only in the "molecular" function.

The main difference between zero and finite k functions is that their time integral is proportional to the viscosities at $k=0$ [Eqs. (2.8) and (2.9)], but it vanishes at finite k due to the conservation law. As a consequence, as Evans pointed out [16], the generalized viscosities cannot be obtained from a Green-Kubo relation at finite k. The discontinuity of the spectra at $\omega=0$ can be observed in Fig. 3. Notice that these spectra are the transforms of the "atomic" $F_{44}(k,t)$ calculated from Eqs. (3.2)–(3.5), so that the small deviation from zero at $\omega=0$ at finite k can be taken as a measure of the accuracy of the calculation. Hence, the generalized viscosities must be obtained from the relevant current or the stress tensor ACF as follows:

$$\tilde{\eta}_L(k,z)=\rho\frac{z-\tilde{G}_{22}(k,z)}{zk^2\tilde{G}_{22}(k,z)}$$

$$=\rho\frac{[f_{un}(k)^2+z^2]\dfrac{\tilde{F}_{44}(k,z)}{V_{22}}-z\dfrac{f_{un}(k)^2}{k^2}}{z\left[z-\dfrac{\tilde{F}_{44}(k,z)k^2}{V_{22}}\right]}\ , \qquad (3.6)$$

$$\tilde{\eta}(k,z)=\rho\frac{1-z\tilde{C}_{\perp}^{(N)}(k,z)}{k^2\tilde{C}_{\perp}^{(N)}(k,z)}=\rho\frac{z\tilde{F}_{44}^{(\perp)}(k,z)}{zC_{\perp}(k,0)-\tilde{F}_{44}^{(\perp)}(k,z)k^2}\ . \qquad (3.7)$$

We remark that Eq. (3.6) is only valid when temperature and density fluctuations are not coupled [$\gamma(k)=c_P(k)/c_V(k)\to 1$ and $|z_{q\sigma}(k,z)|\to 0$].

At finite k's the most practical route to the generalized viscosities is that expressed by the leftmost equalities that rely on currents. At $k=0$, conversely, where the Green-Kubo relations hold, only the rightmost formulas involving the stress tensor can be used, so that $\tilde{\eta}_L(0,z)$ and $\tilde{\eta}(0,z)$ are proportional to the spectrum of the ACF of the relevant components of the stress tensor.

The above mentioned discontinuity does not affect the generalized viscosities. They depend weakly on k, especially in the low-k region. Actually, the $k=0$ and $k=k_{\min}$ data are almost identical; see Fig. 4. In this figure the "atomic" and "molecular" generalized viscosities are reported at some values of k. $\tilde{\eta}_L(k,z)$ turns out to be equal at all frequencies, while $\tilde{\eta}(k,z)$ has a more pronounced high-frequency librational part in the molecular version, as noticed above. In view of the conservation law, the difference in the high-frequency part, hardly visible in the parent $C_{\perp}(k,t)$, becomes more apparent in their spectrum times ω^2, shown in the inset of Fig. 4(b) at some values of k. It is also apparent that the $z=0$ value, i.e., the viscosity, is the same for the atomic and molecular formalism.

In the hydrodynamic limit, the sound attenuation coefficient is $\Gamma/k^2 \propto \eta_L$, when the ratio of specific heats, γ, is very close to 1, as for water in the low-k region [1]. This relation can be extended to finite k, in the spirit of generalized hydrodynamics, by employing the (k,ω)-dependent viscosity discussed above. Hence, a density fluctuation that propagates at $k = k_{\min}$ essentially "feels" a viscosity corresponding to the frequency of the maximum of the sound wave, i.e., 8 THz. This value is much smaller (see Fig. 4) than in the $\omega = 0$ regime relevant to the same wave in the limit $k = 0$. The consequence of this is the large narrowing of the acoustic band at finite k's, compared to its hydrodynamic behavior; see Figs. 15 and 16 of Ref. [1]. This effect is particularly remarkable in the supercooled region, while, as can be seen in Fig. 4(a) and the inset, the drop of viscosity between $\omega = 0$ and the frequency of the acoustic mode is less substantial at 298 K, in agreement with a smaller narrowing of the band.

Finally, we computed separately the CF of the potential and kinetic contributions to σ and found that the CF

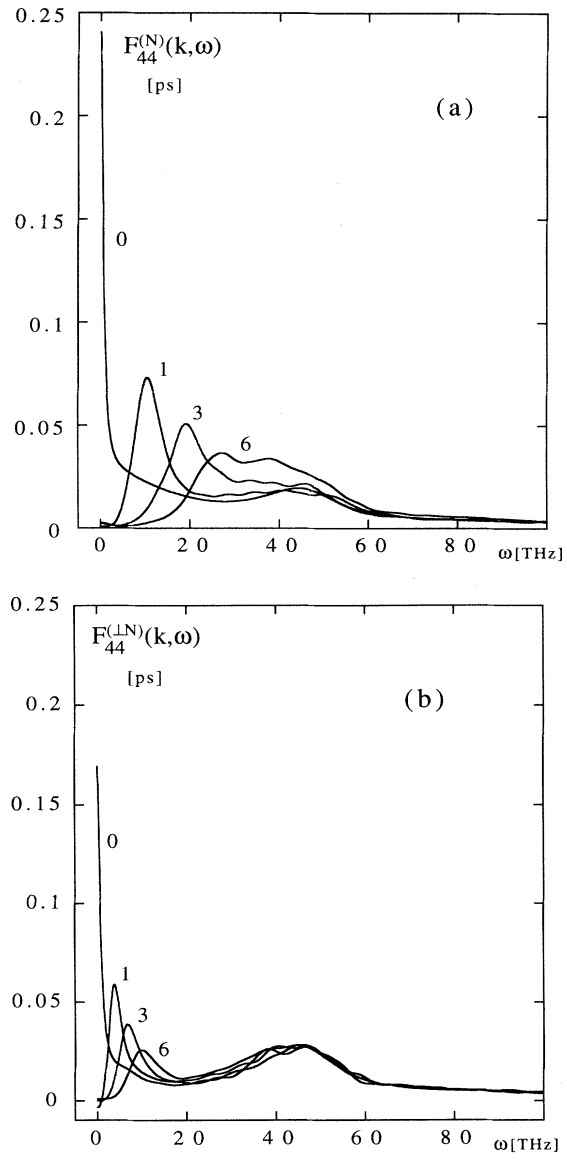

FIG. 3. (a) Spectra of the normalized ACF of the diagonal components of the stress tensor at 245 K. The curves are labeled according to the value of $(k/k_{\min})^2$. (b) The same as (a) for the off-diagonal components. Note that throughout this paper 1 $ps^{-1} = 1$ THz.

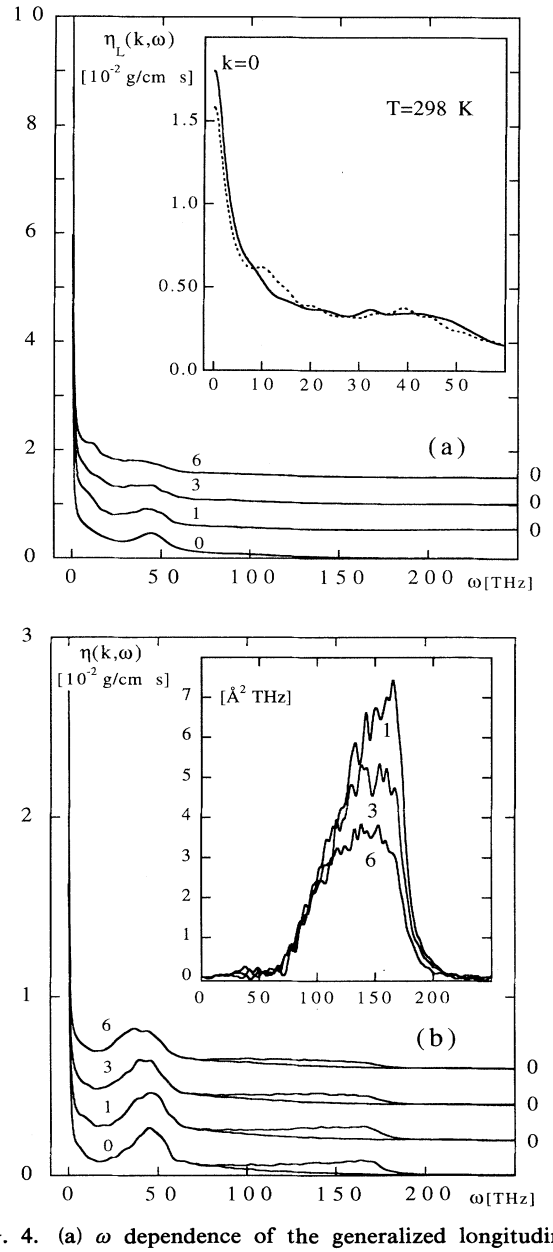

FIG. 4. (a) ω dependence of the generalized longitudinal viscosity at a few values of k [Eq. (3.6)]. The inset shows the same function at 298 K at $k = 0$, full curve, and $k = k_{\min}$, dotted curve. (b) The same as (a) for the shear viscosity [Eq. (3.7)]. The curves are shifted along the vertical axis for clarity. The inset shows $\omega^2[C_\perp^{(m)}(k,\omega) - C_\perp^{(a)}(k,\omega)]/[k^2 C_\perp^{(a)}(k,t=0)]$.

of the potential part accounts for $\approx 99\%$ at $t=0$, at both temperatures and for diagonal and off-diagonal components, while that of the kinetic term decays very fast into the noise.

B. Comparison of MD and hydrodynamic model results for the ACF of the stress tensor

In view of the long runs required to obtain reliable data for collective transport parameters via equilibrium time correlation functions, two MD simulation runs have been carried out at average temperatures of 245 and 298 K, on samples of 343 molecules. The runs were 450 and 370 ps long, respectively, with time steps of 2.5 fs at 245 K and 2.0 fs at 298 K. These runs have led to pressures of -0.3 and -0.1 kbar at 245 and 298 K, while the shorter test run gave -0.16 and -0.19 kbar for "molecular" and "atomic" definition at 245 K. The difference between these data, which should be equal [14,17], is an indication of the statistical uncertainty of the relatively short test run mentioned in Sec. III A.

In these long runs, the stress tensor has been computed at $k=0$ according to the "molecular" definition. In Fig. 5, the normalized MD CF of the diagonal components of the stress tensor is compared with that predicted by extrapolating to $k=0$ the data of Tables V and VIII of Ref. [1]. The same comparison for the CF of the off-diagonal components is shown in Fig. 6. In both figures the librational contribution has been removed from the MD CF's. This contribution is shown separately in the insets together with the total CF's obtained from simulation. Actually, the librational contribution has been extracted from the rest of the CF in the frequency domain, thanks to the clear separation of the frequency scales. An example of this separation at 245 K is shown in Fig. 7. (As in [1], the transform shown has been obtained after writing

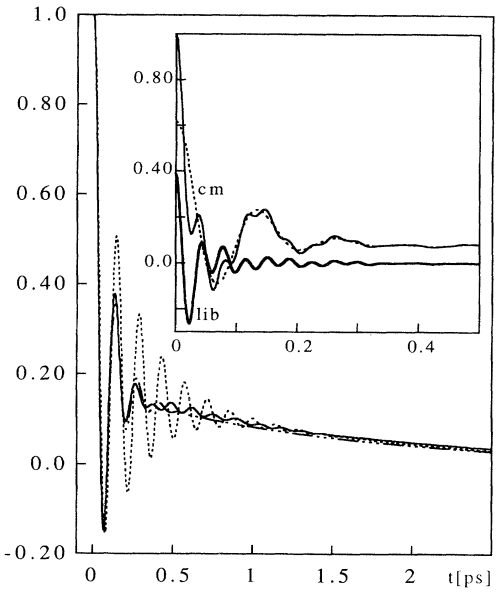

FIG. 6. Same as Fig. 5 for the off-diagonal components of the stress tensor. The dot-dashed curve is obtained from a fit of $\tilde{C}_{\perp}(k,z)$ according to Eq. (3.12).

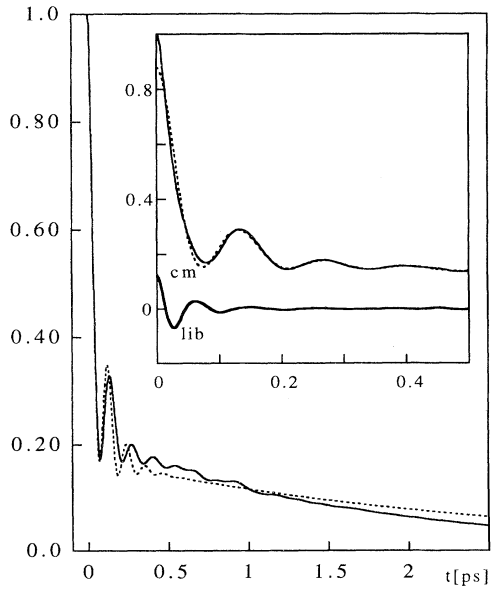

FIG. 5. Comparison of the normalized CF of the diagonal components of the stress tensor obtained from generalized hydrodynamics (dotted curve) and from the simulation (full curve). The librational (lib) contribution has been removed from the latter curve and is shown in the inset with the total CF and the rest (cm). $T=245$ K.

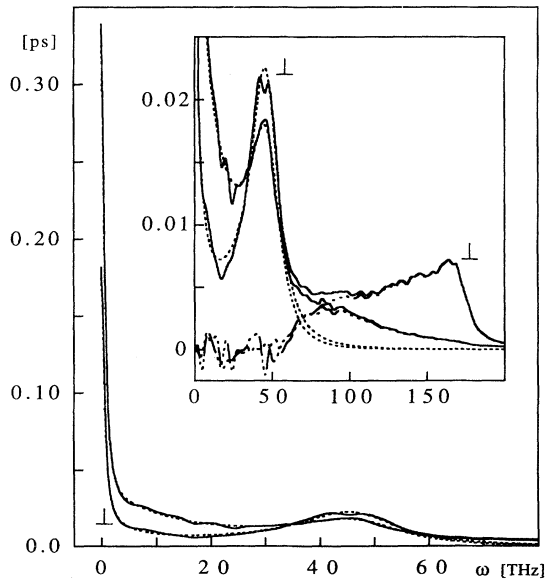

FIG. 7. Spectra of the CF's of the diagonal and off-diagonal ($\perp$) components of the stress tensor at $T=245$ K. The full and dotted curves correspond to simulation CF and a fit based on Eq. (3.12), respectively (see text). The inset shows the higher frequency part of the spectra, with the differences between MD and fitting functions, that are negligible in the low frequency region (dot-dashed curves).

the relevant CF as a sum of a fitting function with a known analytical transform, and a rest that decays fast to zero and is numerically transformed. The two contributions are then added to give the desired transform).

The amplitude of the librational contribution, i.e., the value of the librational part of the total CF at $t=0$, is about 15% and 40% for the diagonal and off-diagonal components, respectively; see the insets of Figs. 5 and 6. These librational contributions also explain the disagreement between the values of $f_{u\sigma}(k)^2$ and $\omega_\perp(k)^2$ obtained from the initial value of the appropriate CF and the second moment of the transverse current CF, and those derived from the fit (see Tables V, VI, VIII, and IX of [1]).

The model introduced in [1] assumes a time dependence of the normalized memory function of the longitudinal current CF, $G_{22}(k,t)$, of the form

$$n_\sigma(k,t)=(1-\alpha_1^{(\sigma)}-\alpha_2^{(\sigma)})e^{-\gamma_3^{(\sigma)}t} \times[\cos(\omega_n^{(\sigma)}t)+m_n^{(\sigma)}\sin(\omega_n^{(\sigma)}t)] +\alpha_1^{(\sigma)}e^{-\gamma_1^{(\sigma)}t}+\alpha_2^{(\sigma)}e^{-\gamma_2^{(\sigma)}t}, \tag{3.8}$$

where $\gamma_1^{(\sigma)}$ and $\gamma_2^{(\sigma)}$ are the decay rates of the fast and slow exponentials that describe the analogy of the collisional regime and the long-time tail, respectively.

$$m_n^{(\sigma)}=\frac{\alpha_1^{(\sigma)}\gamma_1^{(\sigma)}+\alpha_2^{(\sigma)}\gamma_2^{(\sigma)}+(1-\alpha_1^{(\sigma)}-\alpha_2^{(\sigma)})\gamma_3^{(\sigma)}}{\omega_n^{(\sigma)}(1-\alpha_1^{(\sigma)}-\alpha_2^{(\sigma)})} \tag{3.9}$$

and

$$\alpha_2^{(\sigma)}=\frac{2\gamma_3^{(\sigma)}(\omega_n^{(\sigma)2}+\gamma_3^{(\sigma)2})-\alpha_1^{(\sigma)}(\gamma_1^{(\sigma)}+2\gamma_3^{(\sigma)})[\omega_n^{(\sigma)}+(\gamma_3^{(\sigma)}-\gamma_1^{(\sigma)})^2]}{(\gamma_2^{(\sigma)}+2\gamma_3^{(\sigma)})[\omega_n^{(\sigma)2}+(\gamma_3^{(\sigma)}-\gamma_2^{(\sigma)})^2]} . \tag{3.10}$$

In Eqs. (3.9) and (3.10) the k dependence of the parameters is omitted for brevity.

In the frequency domain the above equations correspond to assuming a z dependence of the transform $\tilde{n}_\sigma(k,z)$, such as

$$\tilde{n}_\sigma(k,z)\equiv\frac{1}{z+z_\sigma(k,z)} \equiv\frac{1}{z+J_\sigma(k,0)\dfrac{z^2+a_1(k)z+a_0(k)}{z^3+a_1(k)z^2+b_1(k)z+b_0(k)}} \tag{3.11}$$

$J_\sigma(k,0)$ is the initial value of the memory kernel of $n_\sigma(k,t)$ and has been shown in [1] to be related to the binary collision time. The six parameters that enter Eq. (3.8) can be calculated [1] from the five parameters of Eq. (3.11). Earlier models [4,7] only require three parameters, as they do not include the description of the oscillatory motion of the tagged molecule in the nearest-neighbor cage. This motion, however, turns out to play an important role in the CF's relevant to the stress tensor, and hence in viscosity, and its inclusion in the model demands two additional parameters, which are its frequency $\omega_n^{(\sigma)}$ and decay rate $\gamma_3^{(\sigma)}$.

Equations (3.9) and (3.10) insure that $\dot{n}_\sigma(0,0)$ and $\ddot{n}_\sigma(0,0)=0$, respectively. The latter constraint amounts to imposing that the derivative of the memory kernel of $n_\sigma(k,t)$ also vanish at $t=0$, i.e., $\dot{J}_\sigma(k,0)=0$, and translates into an amplitude of the slow exponential, $\alpha_2^{(\sigma)}$, or of the oscillatory function, $(\alpha_3^{(\sigma)}=1-\alpha_1^{(\sigma)}-\alpha_2^{(\sigma)})$, which is a function of the other five fitting parameters.

The same time dependence as $n_\sigma(k,t)$ has been assumed in [1] for the ACF of transverse memory kernel $n_\perp(k,t)$. As can be seen in Figs. 5 and 6, the agreement between MD and predicted CF's is better in the longitudinal case, while the damping of the "cage mode" is too small in the transverse case. This could be anticipated from the results obtained when fitting the transforms $\tilde{C}_\perp(k,z)$ (see the inset of Fig. 22 of Ref. [1]) and is a consequence of imposing $\ddot{n}_\perp(k,0)=0$ or Eq. (3.11) with too few parameters.

This constraint can be released by letting $a_1(k)\neq b_2(k)$, where a_j and b_j are the coefficients of z^j in the numerator and denominator of $z_\sigma(k,z)$ in Eq. (3.11). The number of parameters would then increase from five to six and the correct short-time behavior would be lost, i.e., $\dot{J}_\perp(k,0)\neq 0$. The latter feature can be maintained, with a satisfactory description of the decay rate, by increasing the degree of the polynomial in z in the numerator and denominator of $z_\sigma(k,z)$ [or $z_\perp(k,z)$], so that

$$z_\perp(k,z) \equiv J_\perp(k,0)\frac{z^3+\bar{a}_2(k)z^2+\bar{a}_1(k)z+\bar{a}_0(k)}{z^4+\bar{a}_2(k)z^3+\bar{b}_2(k)z^2+\bar{b}_1(k)z+\bar{b}_0(k)} . \tag{3.12}$$

Refitting $\tilde{C}_\perp(k,z)$ according to this procedure, we obtain a correct decay rate of the "cage mode," as can be seen in Fig. 6. Moreover, we find that $\bar{a}_2(k)\approx 10^3$ THz, i.e., much larger than the frequency of the "cage mode" and of the libration, so the z^3 and z^4 terms can be neglected in the numerator and denominator of Eq. (3.12), respectively. Dividing both by $\bar{a}_2$, $z_\perp(k,z)$ would again be described as in Eq. (3.11), with parameters scaled by $\bar{a}_2$. So, the coefficients of $n_\perp(k,t)$ can be calcu-

lated as described in the Appendix of Ref. [1], with a time dependence given by Eq. (3.8), but without the constraint expressed by Eq. (3.10).

Table I allows us to compare the fitting parameters obtained from the direct calculation and from the prediction based on the model introduced in Ref. [1]. As already mentioned, this requires an extrapolation to $k=0$ of the values derived from $\tilde{G}_{11}(k,z)$ and $\tilde{G}_{22}(k,z)$ for the longitudinal part [Eqs. (3.8)–(3.11)] and from $\tilde{C}_{\perp}(k,z)$ for the transverse part [Eq. (3.12)].

The agreement between the two sets of data is fair for the longitudinal part and good for the transverse part. This difference probably occurs because it is easier to extract the behavior of the "cage mode" from the data of $\tilde{C}_{\perp}(k,z)$ rather than from $\tilde{G}_{11}(k,z)$ or $\tilde{G}_{22}(k,z)$. The "cage mode" is in fact less separated from the acoustic mode than from the shear one, especially at 298 K [see Figs. 12 and 22 (b) of Ref. [1]). However, the difference between the predicted and MD slopes of the long-time tail in the longitudinal case (Fig. 5) is to be traced back to the fluctuation of the slower part of $F_{11}(k,t)$; see Fig. 21 of Ref. [1]. This might prevent the model, originally based on a subset of the MD data, from reproducing more accurately the long-time tail of this CF. An additional source of error for the model is the extrapolation to $k=0$ of the data obtained at finite k's.

Shear and longitudinal viscosity that has been calculated according to the Green-Kubo relations (2.8) and (2.9) can be compared to that obtained in [1] at both temperatures. As can be seen in Fig. 8, it is necessary to extend the function to times longer than actually observed to ensure convergence of the integral, mainly at 245 K. Equations (2.8), (2.9), and (3.8) indicate that the formula we must use to do this is

$$\varphi(t)=\varphi^{\mathrm{HF}}+\varphi^{\mathrm{LF}}(1-e^{-\gamma_{2\varphi}t}) , \tag{3.13}$$

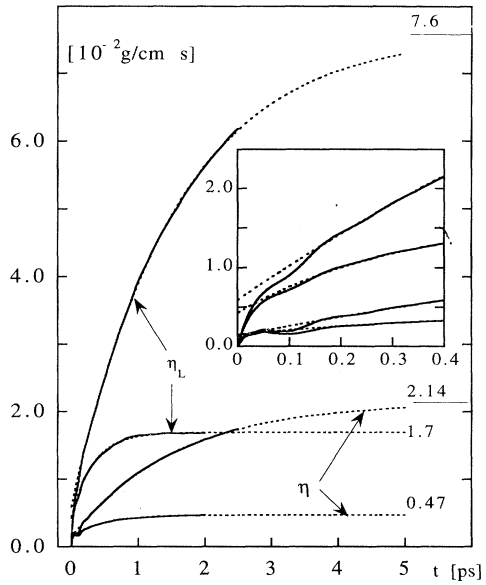

FIG. 8. Running integrals of the CF of diagonal and off-diagonal components of the stress tensor (full curves). Their time extension (doted curves) and asymptotic value has been obtained from a fit based on Eq. (3.13). For both shear and longitudinal viscosity the higher curve corresponds to 245 K and the lower to 298 K. The inset shows a detail of the short time region.

where φ can either be shear or longitudinal viscosity. In Eq. (3.13) φ^{HF} and φ^{LF} represent the contribution of faster and slower dynamics to the integral, respectively. The fits shown in Fig. 8 cover all times beyond 0.2 ps, but it must be noted that the fitting parameters and mainly $\varphi^{\mathrm{HF}}+\varphi^{\mathrm{LF}}$ depend weakly on where the fit starts.

TABLE I. Comparison of the fitting parameters of the normalized (N) CF of the diagonal and off-diagonal components of the stress tensor obtained from generalized hydrodynamics [$G_{44}(0,t)$ and $n_{\perp}(0,t)$] and directly computed [$F^{N}_{44}(0,t)$ and $F^{(\perp N)}_{44}(0,t)$]. The results of columns 2 and 3 are derived from a fit that includes the constraint of the vanishing third derivative of the memory kernel of Eq. (3.8), while for those in parentheses and in the remaining columns this constraint is released. (a) $T=245$ K; (b) 298 K.

	$G_{44}(0,t)$ [2]	$F^{N}_{44}(0,t)$		$n_{\perp}(0,t)$	$F^{(\perp N)}_{44}(0,t)$
		(a)			
$\gamma_1^{(\sigma)}$ (THz)	14.8	18.9 (13.3)	$\gamma_1^{(\perp)}$ (THz)	8.3	6.5
$\gamma_2^{(\sigma)}$ (THz)	0.4	0.62 (0.61)	$\gamma_2^{(\perp)}$ (THz)	0.68	0.60
$\gamma_3^{(\sigma)}$ (THz)	10.9	11.9 (14.6)	$\gamma_3^{(\perp)}$ (THz)	10.4	10.7
$\omega_n^{(\sigma)}$ (THz)	54.3	51.2 (48.5)	$\omega_n^{(\perp)}$ (THz)	45.8	46.6
$\alpha_1^{(\alpha)}$	0.504	0.446 (0.338)	$\alpha_1^{(\perp)}$	0.11	0.10
$\alpha_2^{(\sigma)}$	0.174	0.222 (0.214)	$\alpha_2^{(\perp)}$	0.16	0.16
		(b)			
$\gamma_1^{(\sigma)}$ (THz)	25.4	29.8 (12.2)	$\gamma_1^{(\perp)}$ (THz)	4.8	4.3
$\gamma_2^{(\sigma)}$ (THz)	1.62	2.7 (2.55)	$\gamma_2^{(\perp)}$ (THz)	2.14	2.18
$\gamma_3^{(\sigma)}$ (THz)	25.9	20.6 (22.1)	$\gamma_3^{(\perp)}$ (THz)	16.6	15.2
$\omega_n^{(\sigma)}$ (THz)	65.7	54.8 (46.3)	$\omega_n^{(\perp)}$ (THz)	45.4	45.3
$\alpha_1^{(\sigma)}$	0.716	0.51 (0.272)	$\alpha_1^{(\perp)}$	0.10	0.11
$\alpha_2^{(\sigma)}$	0.10	0.20 (0.163)	$\alpha_2^{(\perp)}$	0.07	0.07

The low-frequency part φ^{LF} is described by the slow exponential, so that $\gamma_{2\varphi} \cong \gamma_2^{(\sigma)}$ (or $\gamma_{2\varphi} \cong \gamma_2^{(\perp)}$) in $n_{\sigma,\perp}(k,t)$, while the higher-frequency part φ^{HF} can be related to the fast exponential, with amplitude $\alpha_1^{(\sigma)}$ (or $\alpha_1^{(\perp)}$) and decay rate $\gamma_1^{(\sigma)}$ (or $\gamma_1^{(\perp)}$) and to the "cage mode," characterized by $\gamma_3^{(\sigma)}$,($\gamma_3^{(\perp)}$) and $\omega_n^{(\sigma)}$,($\omega_n^{(\perp)}$).

At 298 K, the three modes contribute 62%, 23%, and 15% to shear viscosity and 66%, 23%, and 11% to longitudinal viscosity. These figures become 92.5%, 5%, and 2.5% for shear viscosity and 91.5%, 6.7%, and 1.8% for longitudinal viscosity at 245 K. Hence, the contribution of the "cage mode" to viscosity cannot be neglected, especially at 298 K. This mode also causes the oscillation visible in Fig. 8 in the range 0.03–0.15 ps. However, neglecting librational contributions to the integrals produces very minor effects on the off-diagonal components and essentially no effects on the diagonal ones. Actually, there is no difference between curves obtained with or without librational terms beyond 0.2 ps and hence, viscosity does not seem to be affected by this kind of motion.

The behavior of the integral corresponding to bulk viscosity ζ can be obtained by subtracting the shear viscosity curve (times $\frac{4}{3}$) from that of longitudinal viscosity η_L (Fig. 8). The most apparent feature of the resulting curve is a remarkable reduction of the oscillation in the region 0.03–0.15 ps, while the asymptotic value, i.e., ζ, is 4.75×10^{-2} g/cm s at 245 K and 1.07×10^{-2} g/cm s at 298 K. In agreement with the experimental data for water [18,19], these values are roughly twice as large as the corresponding data of shear viscosity reported in Table II. A similar ratio between bulk and shear viscosity is obtained by Wojcik and Clementi [20] and by Kataoka [21] with the Matsuoka-Clementi-Yoshimine (MCY) [22] and related models of water [23]. Moreover, the values in the supercooled region confirm that the TIP4P model also underestimates the increase of viscosity at low temperature, as noticed in [1].

Vortex viscosity that is related to the ACF of the antisymmetric part of the stress tensor cannot be obtained via Green-Kubo integration. Hence, following Evans and Hanley [24], we calculated vortex viscosity from the ACF of the antisymmetric part of the stress tensor and *assuming* a Lorentzian behavior of the low-frequency part of this function. The value we obtain, $(1.9\pm0.4)10^{-3}$ g/cm s, is roughly one order of magnitude smaller than η, while the corresponding data for a Lennard-Jones model of nitrogen are 6.7×10^{-5} g/cm s and 1.13×10^{-3} g/cm s [24,25]. With this procedure the relaxation time τ can also be estimated at 0.08 ± 0.02 ps. This turns out to be very close to that relevant to a Lennard-Jones model of liquid nitrogen, 0.085 ps [24], and much smaller than that obtained from the slope at long time of the stress-stress ACF, namely 1.6 ps; see Table I.

The k dependence of the generalized viscosities, calculated according to Eqs. (3.6) and (3.7), is shown in Fig. 9. As can be seen, the statistical uncertainty is still too large to safely assess if the $k=0$ data are actually smaller than that at $k=k_{\min}$. The overall shape of these curves is similar to that found for hard sphere [26], Lennard-Jones [7], and rubidium liquids [27]. However, bulk viscosity is here much larger than shear viscosity, in contrast to that observed in Lennard-Jones liquids [7]. Also, ζ decays faster than η as a function of k, so that the two curves should merge at about 1 Å^{-1}.

Finally, the infinite frequency shear $G_\infty(k)$ and bulk $K_\infty(k)$, rigidity moduli, and the corresponding relaxation times are reported in Table III as a function of k. The relevant definitions are [28,29]

$$G_\infty(k)=\frac{\rho M}{k_B T}V_{44}^{(1)}(k)=\rho\frac{\omega_\perp(k)^2}{k^2}\ , \tag{3.14}$$

$$K_2\equiv K_\infty-K_0=\frac{\rho M}{9k_B T}\left\langle\sum_\alpha\sum_\beta\sigma^{\alpha\alpha}\sigma^{\beta\beta}\right\rangle\ , \tag{3.15}$$

$$K_0(k)=\frac{Nk_B T}{VS(k)}\ , \tag{3.16}$$

$$\begin{aligned}\rho\frac{\omega_L(k)^2}{k^2}&\equiv-\frac{\rho}{k^2}\lim_{t\to0}\frac{\partial^2 G_{22}(k,t)}{\partial t^2}\\&=\frac{\rho M}{k_B T}V_{44}(k)\\&\approx K_\infty(k)+\frac{4G_\infty(k)}{3}\ .\end{aligned} \tag{3.17}$$

The behavior of $S(k)$ for TIP4P water in the low-k range [1,13] allows us to assume a constant value of $K_0(k)=1.85\times10^{10}$ g/cm s^2. There is a general decrease of the value of the rigidity moduli as a function of k, more apparent for $K_2(k)$ than $G_\infty(k)$.

Unlike transport coefficients, which have been proven to be independent of the formalism adopted, care must be taken in the case of rigidity moduli. We notice that the results of Table III, calculated in the "atomic" formalism, automatically include both translational and rotational degrees of freedom of water, while only translational dynamics is accounted for by the center of mass currents. As a consequence, "molecular" and "atomic"

TABLE II. Longitudinal and shear viscosity obtained from generalized hydrodynamics [1] (columns 2 and 4) and from Green-Kubo integration of the CF's of diagonal and off-diagonal components of the stress tensor (columns 3 and 5). Experimental data [18,19] are in parentheses.

T (K)	$4\eta/3+\zeta$ (10^{-2} g/cm s)	$4\eta/3+\zeta$ (10^{-2} g/cm s)	η (10^{-2} g/cm s)	η (10^{-2} g/cm s)
245	10±2 (27)	7.6±1	2±0.3 (8)	2.14±0.2
298	2±0.5 (3)	1.7±0.25	0.5±0.15 (0.9)	0.47±0.07

TABLE III. Infinite frequency "atomic" shear and bulk moduli and corresponding relaxation times at $T=245$ K. The corresponding data at 298 K are given in the second part of the table. The data in the second column are calculated from the two equilavent definitions of Eq. (3.14). In the third column, the value at $k=0$ has been obtained from Eq. (3.15), while the data in parentheses are calculated from the rightmost part of Eq. (3.17). From the fourth column on, the data in parentheses are experimental results.

k (Å^{-1})	$G_\infty(k)/10^{10}$ (g/cm s^2)	$K_2(k)/10^{10}$ (g/cm s^2)	$G_\infty^{(I)}/10^{10}$ (g/cm s^2)	$K_2^{(I)}/10^{10}$ (g/cm s^2)	τ_η (ps)	τ_ζ (ps)
0	9.5 (9.5)	11.6 (11.0)	1.2 (2.0)[a]	3.1 (4.2)[a]	1.6 (3.2)[b]	1.6 (3.2)[b]
0.288	9.1 (9.4)	(10.3)				
0.498	9.3 (9.1)	(9.3)				
0.705	8.9 (8.9)	(8.0)				
0	8.6 (8.4)	9.2 (9.9)	0.74 (1.36)[a]	1.9 (3.2)[a]	0.46 (.65)[b]	0.4 (0.8)[b]

[a]Reference [32].
[b]Reference [33].

results for $G_\infty(k)$ differ unless the conservation law that links translational currents to pressure tensor is supplemented by an analogous relation between the time dependence of the angular momentum and the couple tensor [25]. For example, at $T=245$ K, in the "molecular" formalism we obtain $G_\infty=12.2\times10^{10}$ instead of 9.5×10^{10} g/cm s^2, and this difference is to be traced back to the rotational terms included only in the "atomic" treatment. Conversely, the molecular K_2 is smaller than the atomic value. Moreover, the agreement between the results obtained for K_2 from Eqs. (3.15) and (3.17) at $k=0$ seems to indicate that water can be considered to interact with central forces [29] in the atomic formalism.

The alternative definition [28] of the shear, $G(\omega)=i\omega\tilde{\eta}(\omega)$, and bulk, $K(\omega)-K_0=i\omega\tilde{\zeta}(\omega)$ modulus allows us to analyze the frequency distribution of the various "modes" that contribute to it, shown in Fig. 10 for both formalisms. Roughly speaking, three frequency regions can be distinguished. The highest frequency, the librational mode, which is more apparent in the molecular function as already mentioned, contributes $\approx20\%$ of the total atomic modulus. The largest part, $\approx60\%$, is provided by the mode centered at 45 THz, the "cage mode." [In the case of K_2 it is the low-frequency dynamics that gives most of the value, i.e., $\approx80\%$, with the remaining $\approx20\%$ due to the cage mode and no contribution from libration]. However, only the slowest mode is in a frequency range that can be matched by experimental ultrasonic measurements. Hence, a sensible comparison of MD and experimental data for shear modulus should be restricted to the contribution of the first band, Table III. It can be seen that there is a fair overall agreement between experimental results and our $G_\infty^{(I)}$ and $K_2^{(I)}$. However, these data confirm that TIP4P water exhibits a faster dynamics than real water at the same temperature. Notice that the infinite frequency values for TIP4P water, as well as other potential models [20,30], would picture water as a liquid more rigid than ice, for which $G_\infty=3.5\times10^{10}$ g/cm s^2 and $K_2=8.7\times10^{10}$ g/cm s^2 [31], at 245 K. This underlines the necessity of comparing experimental data [32] with simulation results in the *same* frequency range, which would restore a more sensible rigidity order, namely TIP4P water, real water and ice. It must also be observed that the use of a rigid model for water might affect the shear and bulk moduli by neglecting vibrational contributions.

Also the relaxation times $\tau_\eta=1/\gamma_2^{(1)}$ and the analogous for bulk viscosity, reported in Table III, are relevant to the first band. It should be stressed that these times depend weakly on k and tend to coincide as temperature is lowered to the supercooled region, as the experimental data do [33]. More importantly, their value, provided they correspond to the dynamics underlying the first band of Fig. 10, can be identified with that obtained by ultrasonic or Brillouin scattering experiments [18,19,32–34].

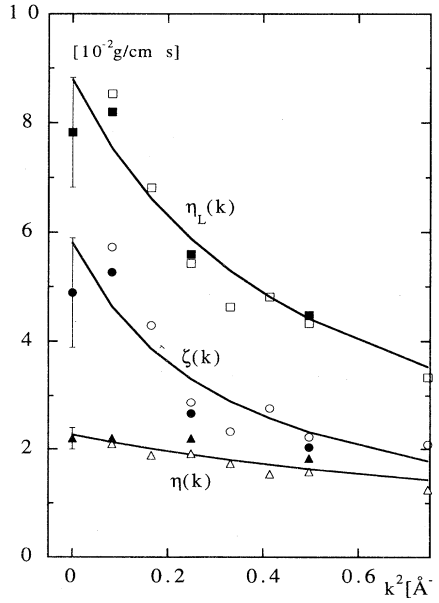

FIG. 9. Generalized shear, $\eta(k)$ (triangles); bulk, $\zeta(k)$ (circles); and longitudinal, $\eta_L(k)$ (squares), viscosity at 245 K. Open symbols: averages on a 166 ps run [1]; filled symbols: averages on a 450-ps run. The curves are drawn as a visual aid.

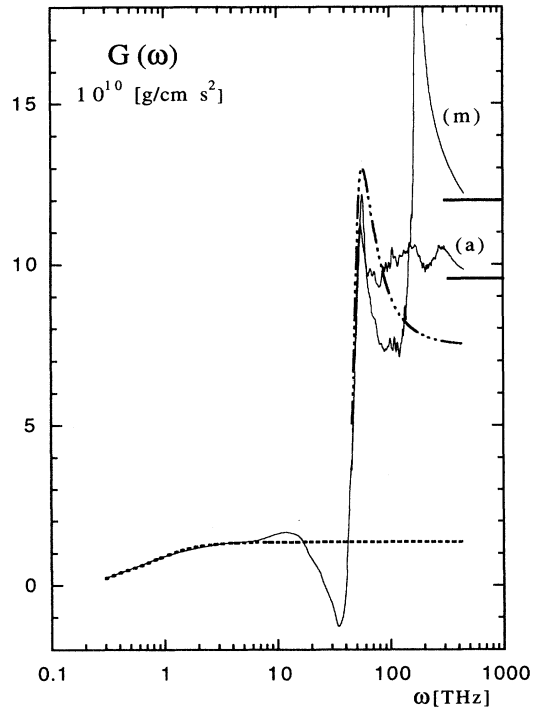

FIG. 10. Frequency dependence of shear modulus at $k=0$ in the atomic (a) and molecular (m) formalism. The horizontal lines on the right indicate the infinite frequency limit according to Eq. (3.14). The dot-dashed curve corresponds to the results of the model defined by the parameters of Table I. The dotted curve is due to the lowest-frequency dynamics (I band) and leads to the value of the TIP4P model used for comparison with experimental data (see text).

As is apparent from Eq. (3.14) and noticed above, $\omega_\perp(k)^2$, which was obtained in [1] from a fit of the molecular transverse currents, is underestimated by $\approx 40\%$ [see Eq. (2.3)] with respect to that obtained from Eq. (2.4). This is due to the use of molecular data (by $\approx 25\%$) and to the librational contribution (by $\approx 15\%$). Librational contributions also determine a value of $f_{u\sigma}(k)^2$ smaller than the computed one by $\approx 15\%$ [see Eq. (2.2)].

IV. SUMMARY AND CONCLUSIONS

In this paper a number of dynamical collective properties of water, modeled by the TIP4P potential, have been studied in the atomic and molecular formalism. We have computed the ACF of the density, longitudinal and transverse currents fluctuations at some finite k's (0.288, 0.498, and 0.705 Å^{-1}) at 245 K. The stress-stress ACF has also been calculated at the same values of k and at $k=0$, again with both formalisms.

The identity of "molecular" and "atomic" results for density, longitudinal currents, and stress tensor ACF support the validity of the "effective" approach adopted to apply extended hydrodynamics to water [1]. As to the ACF of transverse currents and off-diagonal components of stress tensor, the difference between "atomic" and "molecular" results is restricted to the high-frequency region typical of librational dynamics, more apparent in the "molecular" functions.

The main results we have obtained for viscosity can be summarized as follows:

(i) In all cases studied the stress-stress time correlation functions are determined by the potential part of the stress tensor to $\approx 99\%$.

(ii) Both longitudinal and transverse stress-stress ACF's show a fast, oscillatory, initial decay followed by a long-time tail. The latter is more apparent in the shear function at 245 K.

(iii) At $k=0$, the MD longitudinal and shear viscosity of TIP4P water underestimate the experimental data. This defect is shared by other models [20,21]. The disagreement increases in the supercooled region. However, the ratio of 2 between bulk and shear viscosity is correctly reproduced.

(iv) Overall, the k dependence of bulk and shear viscosity is similar to that of hard spheres [26] and Lennard-Jones [7] liquids, with a decrease as a function of k, more apparent for bulk viscosity.

(v) Both shear and bulk viscosity decrease rapidly as a function of ω at the k values considered, and this behavior can be used to account satisfactorily for the substantial narrowing of the acoustic band, compared to the hydrodynamic prediction.

(vi) Vortex viscosity has been estimated to be an order of magnitude smaller than η and some two orders of magnitude larger than vortex viscosity for a Lennard-Jones model of nitrogen [24].

(vii) Unlike viscosities, the values of bulk and shear moduli might depend on the formalism adopted in their calculation, unless the rotational degrees of freedom are included in the molecular formalism, through the couple tensor [25]. The atomic treatment takes all degrees of freedom into account, though it does not separate rotational and translational terms from the outset. We remark, however, that the lowest frequency contribution, the only one that can be sensibly compared to experimental ultrasonic data, does not depend on the definition, being related to the center of mass dynamics.

This set of MD data has also been used to test the results we have obtained for the stress tensor CF's, in an extended hydrodynamics framework, by an extrapolation to $k=0$ of the parameters relevant to a new model of the transport coefficients [1]. Compared to the two-exponential model of Levesque *et al.* [4,7], the new model has the advantage of correctly describing the short-time behavior of the CF's and including the oscillatory local motion (45–50 THz) we have called "cage mode." Thus, the overall agreement between MD and theoretical results is satisfactory and both the general shape of the curves and the "cage mode" oscillation are correctly reproduced. It must be stressed that the contribution of the latter mode to bulk and shear viscosity cannot be neglected, being $\approx 15\%$ of η at 298 K. Its role is even more important for shear and bulk moduli. Librational motions (80–170 THz), however, practically do not affect viscosity; their only effect is a scaling of the amplitude of the memory kernel for shear and longitudinal viscosity,

which leads to underestimating $\omega_\perp(k)^2$ and $f_{u\sigma}(k)^2$ in the fitting process.

There is also a good agreement between computed and predicted shear and longitudinal viscosity, i.e,. the integral of the stress-stress ACF's, at $k=0$. Most of their value is due to the long time tail of the CF's, described by the slow exponential in the model. In this connection, it is worth mentioning that the time dependence of our data is better fitted by an exponential than a power law. An analogous conclusion has been drawn for the Lennard-Jones fluid at the triple point in a much longer simulation study [35]. The best fit exponent we find for the power law is close to $-\frac{3}{2}$ at 298 K and to $-\frac{2}{3}$ at 245 K for both shear and longitudinal function. We recall that the theoretical prediction that leads to the value $-\frac{3}{2}$ is appropriate only for the kinetic part of the viscosity [36], which is negligible in our case. Work is in progress to extend this kind of study to $G_{55}(k,t)$, the CF relevant to the longitudinal heat flux and generalized thermal conductivity.

[1] D. Bertolini and A. Tani, Phys. Rev. E **51**, 1091 (1995).

[2] I. M. de Schepper, E. G. D. Cohen, C. Bruin, J. C. van Rijis, W. Montfrooij, and L. A. de Graaf, Phys. Rev. A **38**, 271 (1988).

[3] W. L. Jorgensen, J. Chandrasekhar, J. D. Madura, R. W. Impey, and M. L. Klein, J. Chem. Phys. **79**, 926 (1983).

[4] D. Levesque, L. Verlet, and J. Kurkijarvi, Phys. Rev. A **7**, 1690 (1973).

[5] J. P. Hansen and I. R. McDonald, *Theory of Simple Liquids* (Academic, London, 1988).

[6] D. Bertolini, P. Grigolini, and A. Tani, J. Chem. Phys. **91**, 1191 (1989).

[7] D. Levesque and L. Verlet, Mol. Phys. **61**, 143 (1987).

[8] P. K. Kahol, R. Bansal, and K. N. Pathak, Phys. Rev. A **14**, 408 (1976).

[9] U. Balucani, G. Ruocco, M. Sampoli, A. Torcini, and R. Vallauri, Chem. Phys. Lett. **209**, 408 (1993).

[10] R. D. Olmsted and R. F. Snider, J. Chem. Phys. **65**, 3407 (1976); **65**, 3423 (1976).

[11] D. J. Evans, Mol. Phys. **32**, 41 (1976); R. Edberg, G. P. Morris, and D. J. Evans, J. Chem. Phys. **86**, 4555 (1987).

[12] M. Allen, Mol. Phys. **52**, 705 (1984).

[13] F. Sciortino and S. Sastry, J. Chem. Phys. **100**, 3881 (1994), and references therein.

[14] G. Marechal and J. P. Ryckaert, Chem. Phys. Lett. **101**, 548 (1983).

[15] M. Ferrario, in *Computer Simulation in Chemical Physics,* edited by M. P. Allen and D. J. Tildesley (Kluwer, Dordrecht, 1993), Chap. 5.

[16] D. J. Evans, Phys. Rev. A **23**, 2622 (1981).

[17] H. J. C. Berendsen, G. Ciccotti, and J. P. Ryckaert, Comput. Phys. Rep. **4**, 345 (1986).

[18] J. Teixeira and J. Leblond, J. Phys. (Paris) **39**, L83 (1978); O. Conde, J. Teixeira, and P. Papon, J. Chem. Phys. **76**, 3747 (1982).

[19] C. A. Angell, in *Water, a Comprehensive Treatise,* edited by F. Franks (Plenum, New York, 1982), Vol. VII.

[20] M. Wojcik and E. Clementi, J. Chem. Phys. **85**, 6085 (1986).

[21] Y. Kataoka, Bull. Chem. Soc. Jpn. **62**, 1421 (1989).

[22] O. Matsuoka, E. Clementi, and M. Yoshimine, J. Chem. Phys. **64**, 1351 (1976).

[23] V. Carravetta and E. Clementi, J. Chem. Phys. **81**, 2646 (1984).

[24] D. J. Evans and H. J. M. Hanley, Phys. Rev. A **25**, 1771 (1982); R. Edberg, G. P. Morris, and D. J. Evans, J. Chem. Phys. **86**, 4555 (1987); D. J. Evans and G. P. Morris, *Statistical Mechanics of Nonequilibrium Liquids* (Academic, London, 1990).

[25] D. J. Evans and W. B. Streett, Mol. Phys. **36**, 161 (1978).

[26] W. E. Alley and B. J. Alder, Phys. Rev. A **27**, 3158 (1983).

[27] U. Balucani, R. Vallauri, and T. Gaskell, Phys. Rev. A **33**, 4263 (1987); **37**, 3386 (1988).

[28] R. Zwanzig, J. Chem. Phys. **43**, 714 (1965); R. Zwanzig and D. Mountain, *ibid.*, **43**, 4464 (1965).

[29] R. Zwanzig, Phys. Rev. **156**, 190 (1967).

[30] A. Rahman and F. H. Stillinger, Phys. Rev. A **10**, 368 (1974).

[31] R. E. Gagnon, H. Kiefte, M. J. Clouter, and E. Whalley, J. Chem. Phys. **89**, 4522 (1988).

[32] W. M. Slie, A. R. Donfor, Jr., and T. A. Litovitz, J. Chem. Phys. **44**, 3712 (1966).

[33] G. D'Arrigo, J. Chem. Phys. **75**, 921 (1981), and references therein.

[34] G. Maisano, P. Migliardo, F. Aliotta, C. Vasi, F. Wanderlingh, and G. D'Arrigo, Phys. Rev. Lett. **52**, 1025 (1984).

[35] M. Ferrario, G. Ciccotti, B. L. Holian, and J. P. Rychaert, Phys. Rev. A **44**, 6936 (1991).

[36] B. J. Alder, *Molecular-Dynamics Simulation of Statistical-Mechanical Systems,* edited by G. Ciccotti and W. G. Hoover (North-Holland, Amsterdam, 1986).